

Quench Dynamics and Hall Response of Interacting Chern Insulators

Michael Schüler,¹ Jan Carl Budich,² and Philipp Werner¹

¹Department of Physics, University of Fribourg, 1700 Fribourg, Switzerland

²Institute of Theoretical Physics, Technische Universität Dresden, 01062 Dresden, Germany

We study the coherent non-equilibrium dynamics of interacting two-dimensional systems after a quench from a trivial to a topological Chern insulator phase. While the many-body wavefunction is constrained to remain topologically trivial under local unitary evolution, we find that the Hall response of the system can dynamically approach a thermal value of the post-quench Hamiltonian, even though the efficiency of this thermalization process is shown to strongly depend on the microscopic form of the interactions. Quite remarkably, the effective temperature of the steady state Hall response can be arbitrarily tuned with the quench parameters. Our findings suggest a new way of inducing and observing low temperature topological phenomena in interacting ultracold atomic gases, where the considered quench scenario can be realized in current experimental set-ups.

Recent experimental progress in realizing topological insulators in a non-equilibrium fashion in ultracold atomic gases [1–6] and periodically driven solids [7, 8] raises fundamental questions regarding the quench dynamics of topological phases. Rather than preparing the ground state of the system of interest, the natural protocol in synthetic material systems is to start from a trivial initial state, and quench the (effective) Hamiltonian into a topological phase before observing the coherent dynamics of the system. In this scenario topological invariants of the many-body state, such as the Chern number, are conserved (remain trivial), as the post-quench time-evolution represents a local unitary transformation [9]. Nevertheless, several observables provide signatures of a change in the topological properties, including circular dichroism in photoabsorption [10–12], characteristic edge currents [13], and the nonequilibrium Hall effect [14–20]. In quenched noninteracting systems, the Hall response – as the archetype of a topological response property – typically exhibits long-lasting oscillations which may be reduced in certain cases by specifically designed quench protocols [21]. In open systems, where the aforementioned constraints on the temporal invariance of topological properties are absent, the Hall response may equilibrate due to extrinsic dephasing [17] or quantum dissipation [11, 22].

The purpose of this work is to consider the quench dynamics of *closed interacting* topological 2D systems, where the time evolution is still unitary at a global level, while two-body scattering provides a source of *intrinsic dissipation* which may enable thermalization processes. In this coherent scenario, it is interesting to investigate which signatures of topology can dynamically equilibrate despite the manifestly trivial character of the time-evolved many-body state. Furthermore, thermalization in a closed quantum system is a complex process, and, depending on the allowed scattering processes, the system may be trapped in a long-lived prethermal state [23–27] in which local observables appear to be thermalized, whereas nonlocal quantities are not. For a 1D system it has recently been shown [28] that the single-particle density matrix (SPDM) can thermalize towards an equilibrium state of a topologically nontrivial post-quench Hamiltonian. However, the dynamical equilibration of natural observables for topological insulators, in particular *two-particle* quantities such as the Hall conductivity

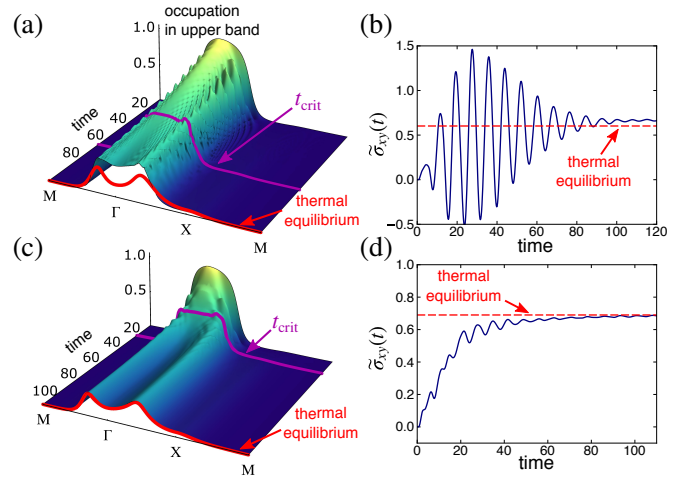


FIG. 1. Thermalization of occupation and Hall response. Upper panels: dynamics of the occupation in the upper band of the post-quench Hamiltonian (a) and corresponding dynamical Hall response $\tilde{\sigma}_{xy}(t)$ (b) in the interacting Chern insulator with local interactions only ($V = 1$). Lower panels: occupation dynamics (c) and build-up of the Hall response (d) in the Chern insulator including nonlocal interactions ($V_0 = 1, V_1 = 0.25V_0$). The results have been obtained within the GKBA, using a $N_k = 220 \times 220$ grid sampling of the BZ.

ity in 2D systems, has remained a largely unexplored question.

Below, we investigate the post-quench dynamics of the Hall response in interacting 2D fermionic systems. With fully microscopic numerical simulations based on the time-dependent nonequilibrium Green’s functions (NEGF) approach [29–31], we demonstrate that a dynamical equilibration to a *thermal* value of the Hall response is possible, if sufficiently many scattering channels are available, while thermalization bottlenecks related to the topological character of the considered quenches result in slow dynamics (see Fig. 1). Specifically, when considering a minimal model system for a Chern insulator, nearest neighbor interactions are necessary to efficiently thermalize the Hall response, even though onsite interactions already render the system non-integrable.

Topological Hubbard model. – We study interacting topological insulator (TI) models on a 2D square lattice with unit lattice constant, defined by the Hamiltonian $\hat{H} = \hat{H}_{\text{TI}} + \hat{H}_{\text{int}}$.

We consider two scenarios for the free Hamiltonian \hat{H}_{TI} : (i) a spinless Chern insulator defined by $\hat{H}_{\text{TI}} = \sum_{\mathbf{k}} \hat{\mathbf{c}}_{\mathbf{k}}^\dagger \mathbf{h}(\mathbf{k}) \hat{\mathbf{c}}_{\mathbf{k}}$ with $\mathbf{h}(\mathbf{k}) = (M - \cos(k_x) - \cos(k_y))\sigma_z + \lambda \sin(k_x)\sigma_x + \lambda \sin(k_y)\sigma_y$. Here, the $\hat{\mathbf{c}}_{\mathbf{k}}^{(\dagger)} = (\hat{c}_{\mathbf{k}E}^{(\dagger)}, \hat{c}_{\mathbf{k}H}^{(\dagger)})$ denote the fermionic annihilation (creation) operators with respect to the underlying two orbitals, labelled by E and H, respectively, in analogy to the original Bernevig-Hughes-Zhang (BHZ) [32] model for HgTe, the σ_i are the Pauli matrices in the orbital pseudospin space, and the lattice momentum \mathbf{k} is defined in the first Brillouin zone (BZ). (ii) A spinful quantum spin Hall insulator with time-reversal symmetry defined by [32] $\hat{H}_{\text{TI}} = \sum_{\mathbf{k}, \sigma} \hat{\mathbf{c}}_{\mathbf{k}, \sigma}^\dagger \mathbf{h}_\sigma(\mathbf{k}) \hat{\mathbf{c}}_{\mathbf{k}, \sigma}$ with $\mathbf{h}_\uparrow(\mathbf{k}) = \mathbf{h}(\mathbf{k})$, $\mathbf{h}_\downarrow(\mathbf{k}) = [\mathbf{h}(-\mathbf{k})]^*$. In both cases, the system is a trivial band insulator for $M < -2$, while $-2 < M < 0$ corresponds to a (spin) Chern insulator with (spin) Chern number $C = 1$. In what follows, all energies (times) are measured in units of the hopping (inverse hopping).

Post-quench dynamics with interactions.— To gain insights into the dynamical manifestation of topological properties, the system is prepared in a low-temperature equilibrium state in the topologically trivial phase. At times $t = 0_+$, the mass parameter M is suddenly switched (continuous ramps of M will be considered further below) to the topological regime and kept constant for $t > 0$. To disentangle scattering processes in the post-quench dynamics from the initial state, \hat{H}_{int} is also switched on suddenly at $t = 0_+$. This protocol can be realized experimentally in ultracold atomic gases by tuning a magnetic field in the vicinity of a Fano-Feshbach resonance [33, 34]. We will consider weak to intermediate inter-particle interactions in this work, so that the topological character of the system is determined by \hat{H}_{TI} .

The time-dependent NEGF approach [29–31, 35] will be used to describe the *correlated* dynamics. This method is based on solving the Kadanoff-Baym equations (KBEs) for the single-particle Green's function (SPGF), from which the SPDM $\rho_\sigma(\mathbf{k}; t)$ and thus all single-particle observables can be computed. The KBEs yield, in principle, the exact SPGF, provided the self-energy kernel is known. In practice however, additional approximations are inevitable. In this work, we employ the second-Born approximation (2BA) to the self-energy, which corresponds to a second-order expansion in the two-body interaction. The 2BA has been shown to provide an excellent description of the electronic structure and dynamics for relatively weak interactions [36, 37].

In order to extrapolate to the thermodynamic limit, the number of points \mathbf{k} sampling the BZ has to be chosen sufficiently large, which – due to the substantial numerical effort of solving the full KBEs – poses a computational challenge. Invoking the generalized Kadanoff-Baym ansatz (GKBA) [38] is an additional approximation which reduces the numerical effort significantly [39]. The GKBA has been shown to yield excellent results in the weak-coupling regime for single-particle observables [36, 40–43]. How well nonequilibrium response properties are captured is less understood and will be addressed in the context of the Hall response below. Both the full KBE and the GKBA treatment conserve the total energy. Therefore, com-

paring the energy of the system after the quench to the thermal equilibrium energies of post-quench interacting system allows to determine the effective temperature T_{eff} and corresponding thermalized observables.

Chern insulator with local interactions.— As the first paradigmatic example we consider the case where \hat{H}_{TI} defines a spinless Chern insulator for $M < -2$. Restricting to local interactions, we consider the interaction term

$$\hat{H}_{\text{int}} = \frac{V}{2} \sum_i \sum_{\alpha \neq \alpha'} \hat{n}_{i,\alpha} \hat{n}_{i,\alpha'}, \quad (1)$$

where i runs over all lattice sites, while $\alpha, \alpha' \in \{E, H\}$. In the following, we fix $\lambda = 0.4$ and consider the quench of the gap parameter $M_{\text{pre}} \rightarrow M_{\text{post}}$ with $M_{\text{pre}} = -3.5$ and $M_{\text{post}} = -1$.

Without band hybridization ($\lambda = 0$), the E and H bands possess a $U(1)$ symmetry, which results in individually conserved particle numbers n_E and n_H . As a result, inter-orbital (and thus inter-band) thermalization will be completely suppressed. In the case $\lambda > 0$ and $C = 1$, inter-orbital scattering in the lower and upper band becomes possible, albeit only active close to the avoided crossings. Furthermore, the non-vanishing Chern number implies that even within the same Bloch band, there are states with opposite orbital character which are not connected by the intra-orbital interaction. Therefore, thermalization can only proceed via higher-order scattering processes.

The expectation of slow thermalization is confirmed by inspecting the time evolution of the occupation in the upper band $f_+(\mathbf{k}; t) = \phi_{\mathbf{k},+}^\dagger \rho(\mathbf{k}; t) \phi_{\mathbf{k},+}$ with respect to the post-quench free Hamiltonian $\mathbf{h}(\mathbf{k}) \phi_{\mathbf{k},\pm} = \varepsilon_\pm(\mathbf{k}) \phi_{\mathbf{k},\pm}$, presented in Fig. 1(a) along the path M– Γ –X–M in the BZ for $V = 1.0$. Initially, the SPDM is prepared as the equilibrium state of the band insulator with dominant E orbital character; quenching M leads to a band inversion with preserved occupation of the E orbital, which after the quench has large weight in the upper band near the center of the BZ. The subsequent relaxation due to particle-particle scattering reduces the number of excited carriers. Computing the injected energy and comparing to thermal equilibrium yields the effective temperature T_{eff} . The corresponding equilibrium occupation $f_+^{\text{eq}}(\mathbf{k}; T_{\text{eff}})$ is represented by the red line in Fig. 1(a). The deviation of $f_+(\mathbf{k}; t)$ from $f_+^{\text{eq}}(\mathbf{k}; T_{\text{eff}})$ illustrates the very slow approach to thermal equilibrium after the quench. Furthermore, the oscillations of the occupation indicate a coherent superposition of the lower and upper band, which is only slowly damped; hence, dephasing exists but is ineffective.

To probe the dynamical Hall response $\tilde{\sigma}_{xy}(t)$, we apply a weak electric field $E_y(t) = F_0(1 - e^{-t/\tau})$ in the y -direction ($F_0 = 10^{-3}$ and $\tau = 5$). Measuring the induced current in the x -direction $J_x(t)$ yields the Hall response $\tilde{\sigma}_{xy}(t) = J_x(t)/F_0$. Figure 2 shows $\tilde{\sigma}_{xy}(t)$ for $V = 0.65$ (a) and $V = 1.0$ (b) [also shown in Fig. 1(b)]. For $V = 0.65$, strong coherent oscillations around a nonthermal value of the Hall conductance dominate and the relaxation to a steady state $\tilde{\sigma}_{xy}(t) \rightarrow \sigma_{xy}(t \rightarrow \infty)$ cannot be observed on the accessible timescales. Increasing

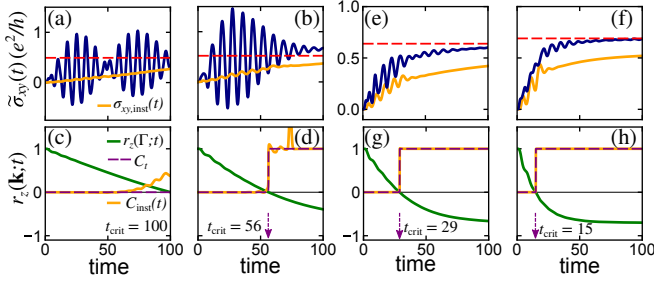


FIG. 2. Dynamics of the Hall response and orbital pseudospin for a Chern insulator with local interactions only ((a)–(d)) and with nonlocal interactions ((e)–(h)). The interaction strength is $V = 0.65$ ((a) and (c)) and $V = 1.0$ ((b) and (d)) in the local case, while for the model with nonlocal interactions it is $V_0 = 0.65$ ((e) and (g)) and $V_0 = 1.0$ ((f) and (h)). We used the GKBA and show results for $N_k = 220 \times 220$ grid points in the BZ.

the interaction strength to $V = 1.0$, a steady state begins to form at times $t \approx 100$; however, its Hall conductance deviates from the thermal equilibrium value, which is consistent with the nonthermal distribution (Fig. 1(a)).

Further insight into the topological properties of the SPDM can be gained by extracting the pseudospin vector $\mathbf{r}(\mathbf{k}; t)$ via the relation $\rho(\mathbf{k}; t) = [I - \mathbf{r}(\mathbf{k}; t) \cdot \boldsymbol{\sigma}]/2$. As long as $\mathbf{r}(\mathbf{k}; t) \neq 0$, the SPDM can formally be expressed as $\rho(\mathbf{k}; t) = \exp(-\mathbf{h}_{\text{aux}}(\mathbf{k}; t))$ with a gapped auxiliary Hamiltonian $\mathbf{h}_{\text{aux}}(\mathbf{k}; t)$. Closing of the gap of $\mathbf{h}_{\text{aux}}(\mathbf{k}; t)$, known from open systems as a purity gap closing [44, 45], marks a dynamical topological transition at the critical time t_{crit} corresponding to $\mathbf{r}(\Gamma; t_{\text{crit}}) = 0$ [46]. The occurrence of the band inversion indicated by $r_z(\Gamma; t)$ passing through zero also allows to define a simplified topological index C_t via $(-1)^{C_t} = \text{sign}(r_z(\Gamma; t)r_z(X; t))$ [47]. This index is plotted together with $r_z(\Gamma; t)$ in Fig. 2(c)–(d). One finds a purity gap closing at $t_{\text{crit}} \approx 100$ for $V = 0.65$ and $t_{\text{crit}} \approx 56$ for $V = 1.0$. Fig. 1(a) shows the distribution $f_+(\mathbf{k}; t_{\text{crit}})$, which changes its curvature at $\mathbf{k} = \Gamma$ at $t = t_{\text{crit}}$, indicating a band inversion. Further analysis [48] shows a decrease of t_{crit} proportional to $V^{-3/2}$.

The pseudospin structure furthermore allows to define the instantaneous Berry curvature

$$\Omega(\mathbf{k}; t) = -\frac{1}{2} \hat{\mathbf{f}}(\mathbf{k}; t) \cdot \left(\frac{\partial \hat{\mathbf{f}}}{\partial k_x} \times \frac{\partial \hat{\mathbf{f}}}{\partial k_y} \right), \quad (2)$$

where $\hat{\mathbf{f}}(\mathbf{k}; t) = \mathbf{r}(\mathbf{k}; t)/|\mathbf{r}(\mathbf{k}; t)|$. The Berry curvature (2) defines the instantaneous Chern number of the SPDM $C_{\text{inst}}(t) = (1/2\pi) \int_{\text{BZ}} d\mathbf{k} \Omega(\mathbf{k}; t)$ and the instantaneous Hall conductance $\sigma_{xy, \text{inst}}(t) = \int_{\text{BZ}} d\mathbf{k} |\mathbf{r}(\mathbf{k}; t)| \Omega(\mathbf{k}; t)$. Importantly, $C_{\text{inst}}(t)$ would be pinned to zero in a noninteracting system. In contrast, Fig. 2(c)–(d) shows a nonzero instantaneous Chern number, which for $V = 1.0$ becomes almost identical to C_t [49]. The instantaneous Hall conductance exhibits a fast increase for $t < t_{\text{crit}}$ and a saturation after $t > t_{\text{crit}}$. However, $\sigma_{xy, \text{inst}}(t)$ does not coincide with the thermal Hall conductance of the interacting system.

Chern insulator with nonlocal interactions.– The thermalization process changes substantially if nonlocal interactions are included. For the purpose of this study, we consider

$$\hat{H}_{\text{int}} = \frac{1}{2} \sum_{i,j} \sum_{\alpha,\alpha'} V_{i,j}^{\alpha\alpha'} \hat{n}_{i,\alpha} \hat{n}_{i,\alpha'}. \quad (3)$$

Here, the interactions are $V_{i,i}^{\alpha\alpha'} = V_0(1 - \delta_{\alpha\alpha'})$ and $V_{i,j}^{\alpha\alpha'} = V_1$ if i and j are nearest neighbours. The nonlocal repulsion is fixed to $V_1 = 0.25V_0$.

Figure 1(c) depicts the occupation of the upper band (with respect to the post-quench free Hamiltonian) $f_+(\mathbf{k}; t)$ for $V_0 = 1.0$. In contrast to the model with local interactions only, the nonlocal part of the interaction includes inter-orbital and intra-orbital scattering, which results in a rapid thermalization of $f_+(\mathbf{k}; t)$ to the equilibrium $f_+^{\text{eq}}(\mathbf{k})$. Furthermore, coherent oscillations are suppressed, indicating pronounced dephasing. The nonequilibrium Hall response is shown in Fig. 2(e)–(f) for $V_0 = 0.65$ and $V_0 = 1.0$, respectively. In this set-up, $\tilde{\sigma}_{xy}(t)$ approaches the thermal equilibrium value within the numerically accessible time window. Furthermore, it shows a qualitatively very similar behavior as the instantaneous conductance $\sigma_{xy, \text{inst}}(t)$, indicating strong dephasing. There are two different regimes: a rapid increase with superimposed oscillations for $t < t_{\text{crit}}$ and a smooth saturation for $t > t_{\text{crit}}$. This behavior of $\sigma_{xy, \text{inst}}(t)$ is also reflected in $\tilde{\sigma}_{xy}(t)$. The time scale of the purity gap closing (Fig. 2(g)–(f)) is significantly shorter as compared to the case with local interactions only: $t_{\text{crit}} \approx 29$ for $V_0 = 0.65$ and $t_{\text{crit}} \approx 15$ for $V_0 = 1.0$. The sign of the curvature of the distribution $f_+(\Gamma; t)$ changes at $t = t_{\text{crit}}$ (Fig. 1(c)). Again, t_{crit} scales as $V^{-3/2}$.

Quantum spin Hall insulator.– Including the spin degree of freedom while requiring time-reversal symmetry gives rise to a \mathbb{Z}_2 quantum spin Hall insulator. This is the typical scenario in materials where the spin-orbit interaction is the mechanism behind the topological gap opening. In this case, the on-site Hubbard repulsion (which is excluded by the Pauli principle in the spinless case) becomes the simplest possible interaction term [50]. For the sake of consistency with the previous discussion, we also include a local inter-orbital coupling and define the interaction term as

$$\hat{H}_{\text{int}} = U \sum_{i,\alpha} \hat{n}_{i,\alpha,\uparrow} \hat{n}_{i,\alpha,\downarrow} + \frac{V}{2} \sum_{i,\sigma} \sum_{\alpha \neq \alpha'} \hat{n}_{i,\alpha,\sigma} \hat{n}_{i,\alpha',\sigma}. \quad (4)$$

We employ the same quench protocol as above and fix $M_{\text{pre}} = -3.5$ and $M_{\text{post}} = -1.5$.

Inspecting the occupation in the upper band for weak ($U = 1.0$, Fig. 3(a)) and slightly increased ($U = 1.5$, Fig. 3(b)) Hubbard repulsion, one finds rapid dephasing and thermalization. Hence, the on-site intra-orbital interaction is sufficient to fully thermalize the system on short time scales (determined by the interaction strength). Adding the inter-orbital coupling V does not change this behavior, albeit the thermalization becomes slightly slower. This is a mean-field effect: the inter-orbital interaction increases the effective post-quench gap parameter $M_{\text{post}}^{\text{eff}} = M_{\text{post}} - Un_E - 2Vn_H + V\rho_{EH}$, where ρ_{EH}

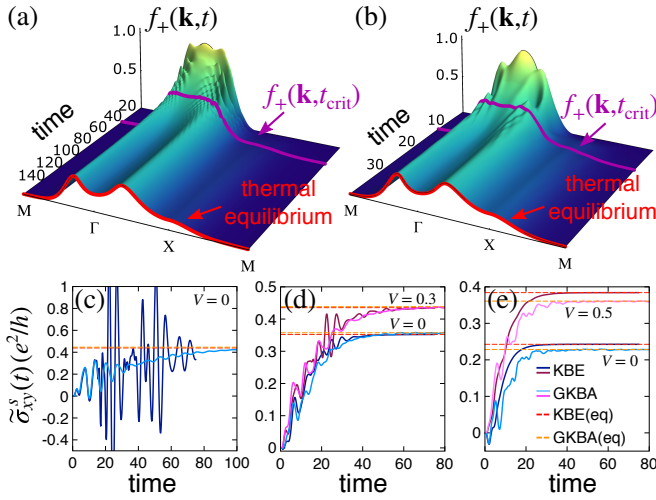


FIG. 3. Dynamics of the occupation $f_+(\mathbf{k}; t)$ in the upper band of a quantum spin Hall insulator for (a) $U = 1.0, V = 0$, and (b) $U = 1.5, V = 0$. The results have been obtained employing the GKBA. The lower panels depict the nonequilibrium spin Hall conductance for (c) $U = 1.0$, (d) $U = 1.5$, and (e) $U = 2.0$.

denotes the off-diagonal element of the local density matrix. This Fock term thus leads to an effectively reduced quench size $M_{\text{post}}^{\text{eff}} - M_{\text{pre}}$, which injects less energy into the system, thus giving rise to slower thermalization. A systematic analysis for different M_{pre} and M_{post} [48] confirms this picture.

While the total Hall conductance vanishes in the spin Chern insulator, the spin Hall conductance $\tilde{\sigma}_{xy}^s(t) = [\tilde{\sigma}_{xy}^\uparrow(t) - \tilde{\sigma}_{xy}^\downarrow(t)]/2$ becomes quantized to one at zero temperature, due to the presence of a $U(1)$ spin rotation symmetry. The spin Hall conductance is presented in Fig. 3(c)–(e). Within the GKBA on a $N_k = 200 \times 200$ grid, which corresponds to the converged thermodynamic limit in all cases, $\tilde{\sigma}_{xy}^s(t)$ rises rapidly and approaches the thermal equilibrium value at the corresponding effective temperature T_{eff} . As for the Chern insulator, the characteristic time scale for the build-up of the spin Hall effect is the critical time t_{crit} of the purity gap closing (also indicated in Fig. 3(a)–(b)). Increasing the strength of the Hubbard repulsion (while keeping $V = 0$) leads to significantly enhanced dephasing, while the steady-state spin Hall conductance σ_{xy}^s is reduced. This can again be attributed to the increase of injected energy due to a stronger effective quench. Including the inter-orbital interaction V counter-acts this effect and thus results in a larger σ_{xy}^s . Hence, tuning the inter-orbital coupling V provides a way of effectively cooling down the system and thus increasing σ_{xy}^s .

It is interesting to compare the GKBA to the full solution of the KBEs (darker lines in Fig. 3(c)–(e)). Due to the numerical effort, the KBE simulations are limited to a 32×32 cluster here. For $U = 1.0$, the GKBA and KBE results agree well up to $t \approx 15$; for later times, finite-size effects dominate the KBE dynamics. Nevertheless, the steady-state σ_{xy}^s agrees well. For the slightly larger interaction $U = 1.5$ (Fig. 3(d)), where dephasing is significantly enhanced and finite-size ef-

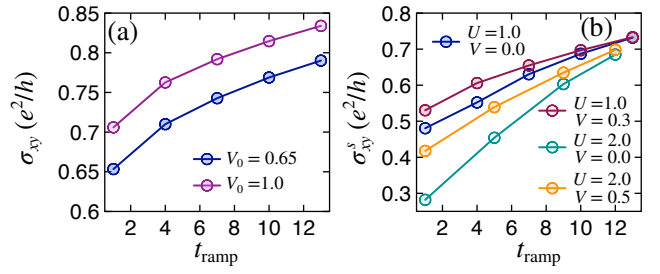


FIG. 4. Steady-state (spin) Hall conductance of (a) the spinless Chern insulator with nonlocal interactions ($V_1 = 0.25V_0$), and (b) the spinful \mathbb{Z}_2 insulator as a function of the ramp time. The GKBA has been used in (a) and (b) for all results, except for $U = 2.0$, where the KBE result is shown.

fects thus suppressed, the GKBA and KBE dynamics agree well, as does the steady state. For stronger interaction, however, deviations become apparent (Fig. 3(e)). The KBE dynamics (which has already converged to the thermodynamic limit) shows much more pronounced dephasing and smoothly approaches the thermal steady state. While the GKBA is also thermodynamically consistent, it seems to underestimate the KBE Hall conductance. Analyzing the Hall conductance in thermal equilibrium [48], we find that the GKBA fails to reproduce the integer Hall effect for $T \rightarrow 0$ [51]. Apart from this subtlety, for moderate interaction strength $U \lesssim 1.5$, the GKBA and KBE treatments agree very well. Since the exact solution is typically in between [52], this comparison establishes the GKBA as an excellent method in the weak-interaction regime, and demonstrates the predictive power of our approach.

Realizing a low-temperature topological state.– The largest steady-state values σ_{xy} (σ_{xy}^s) for the Chern (spin Chern) insulator are around $\sigma_{xy} \simeq 0.68$ and $\sigma_{xy}^s \simeq 0.41$, respectively, corresponding to a high-temperature state after thermalization. The effective temperature can, however, be lowered significantly by slowly *ramping* M . We demonstrate this behavior by modifying our protocol to: (i) preparing the band-insulating system in equilibrium including \hat{H}_{int} , and (ii) modifying the gap according to $M(t) = M_{\text{pre}} + (M_{\text{post}} - M_{\text{pre}})f(t/t_{\text{ramp}})$ [53]. t_{ramp} defines the ramp duration ($M(t_{\text{ramp}}) = M_{\text{post}}$). Figure 4(a) ((b)) shows the steady-state (spin) Hall conductance for various values of the interaction strength. As Fig. 4 demonstrates, the thermal Hall effect can be significantly enhanced for all interactions by increasing t_{ramp} . Slower ramps lead to an adiabatic time evolution for more and more points in the BZ except for the region close to the gap closing at the Γ point. Therefore, the ability of the system to thermalize results in an arbitrarily low T_{eff} and a σ_{xy} or σ_{xy}^s approaching one. This, however, would not be the case for the nonthermal Chern insulator with local interactions only.

Conclusions.– We have systematically investigated the post-quench dynamics of closed interacting two-dimensional topological insulators. We showed that the system can dynamically approach thermal equilibrium with respect to the topological properties of the SPDM and the Hall response,

even though the topological invariant of the many-body state stays pinned to the trivial value. Thus, our results demonstrate that the eigenstate thermalization hypothesis also applies to topologically constrained unitary time evolution. The microscopic scattering mechanisms play a crucial role: while the spin-less Chern insulator with local interactions only is non-integrable, it thermalizes very slowly due to topological restrictions. In contrast, including intra-orbital coupling by nonlocal interactions or extending to a spinfull \mathbb{Z}_2 topological insulator accelerates the thermalization on the one- and two-particle level. Therefore, switching from the topologically trivial to the nontrivial regime by slow ramps allows to realize a low-temperature state with almost integer Hall conductance, providing a new way of dynamically inducing and observing topological phenomena.

This work was supported by the Swiss National Science Foundation through NCCR MARVEL and the European Research Council through ERC Consolidator Grant 724103. The calculations have been performed on the Beo05 cluster at the University of Fribourg, and the Piz Daint cluster at the Swiss National Supercomputing Centre (CSCS).

Appendix: Theoretical methods

Time-dependent nonequilibrium Green's function approach

The time-dependent nonequilibrium Green's function (TD-NEGF) method is based on solving the Kadanoff-Baym equations (KBEs) for the single-particle Green's function (SPGF):

$$(i\partial_t - \mathbf{h}(\mathbf{k}; t)) \mathbf{G}(\mathbf{k}; t, t') = \delta_C(t, t') + \int_C d\bar{t} \mathbf{\Sigma}(\mathbf{k}; t, \bar{t}) \mathbf{G}(\mathbf{k}; \bar{t}, t'). \quad (5)$$

The time arguments of the SPGF $\mathbf{G}(\mathbf{k}; t, t')$ lie on the L-shaped Kadanoff-Baym contour C . In practice, we solve this equation by introducing a set of two-time correlators [31]. The resulting KBEs are

$$i\partial_t \mathbf{G}^>(\mathbf{k}; t, t') = \mathbf{h}(\mathbf{k}; t) \mathbf{G}^>(\mathbf{k}; t, t') + [\mathbf{\Sigma}(\mathbf{k}) * \mathbf{G}(\mathbf{k})]^>(t, t'), \quad (6a)$$

$$-i\partial_t \mathbf{G}^<(\mathbf{k}; t', t) = \mathbf{G}^>(\mathbf{k}; t', t) \mathbf{h}(\mathbf{k}; t) + [\mathbf{G}(\mathbf{k}) * \mathbf{\Sigma}(\mathbf{k})]^<(t', t), \quad (6b)$$

$$i\partial_t \mathbf{G}^{\parallel}(\mathbf{k}; t, \tau) = \mathbf{h}(\mathbf{k}; t) \mathbf{G}^{\parallel}(\mathbf{k}; t, \tau) + [\mathbf{\Sigma}(\mathbf{k}) * \mathbf{G}(\mathbf{k})]^{\parallel}(t, \tau). \quad (6c)$$

Here, the standard Langreth rules [31] define the convolution

$$\begin{aligned} [\mathbf{A}(\mathbf{k}) * \mathbf{B}(\mathbf{k})]^{\gtrless}(t, t') &= \int_0^{t'} d\bar{t} \mathbf{A}^{\mathbf{R}}(\mathbf{k}; t, \bar{t}) \mathbf{B}^{\gtrless}(\mathbf{k}; \bar{t}, t') \\ &+ \int_0^{t'} d\bar{t} \mathbf{A}^{\gtrless}(\mathbf{k}; t, \bar{t}) \mathbf{B}^{\mathbf{A}}(\mathbf{k}; \bar{t}, t') \\ &- i \int_0^{\beta} d\tau \mathbf{A}^{\parallel}(\mathbf{k}; t, \tau) \mathbf{B}^{\parallel}(\mathbf{k}; \tau, t') \end{aligned}$$

and

$$\begin{aligned} [\mathbf{A}(\mathbf{k}) * \mathbf{B}(\mathbf{k})]^{\parallel}(t, \tau) &= \int_0^t d\bar{t} \mathbf{A}^{\mathbf{R}}(\mathbf{k}; t, \bar{t}) \mathbf{B}^{\parallel}(\mathbf{k}; \bar{t}, \tau) \\ &+ \int_0^{\beta} d\tau' \mathbf{A}^{\parallel}(\mathbf{k}; t, \tau') \mathbf{B}^{\mathbf{M}}(\mathbf{k}; \tau' - \tau). \end{aligned}$$

For a given choice of the many-body self-energy $\mathbf{\Sigma}(\mathbf{k})$, one first obtains for the Matsubara SPGF $\mathbf{G}^{\mathbf{M}}(\mathbf{k}; \tau)$ which captures initial correlations. With the initial conditions thus determined, the KBEs (6) govern the real-time evolution.

For the quench setup employed in the main text, the KBEs (6) simplify due to the lack of initial correlations, leading to $\mathbf{\Sigma}^{\parallel}(\mathbf{k}; t, \tau) = 0$. In this scenario, the initial conditions (keeping track of orbital and spin indices) are determined by

$$\begin{aligned} G_{\alpha\alpha'\sigma}^<(\mathbf{k}; 0, 0) &= i\tilde{\rho}_{\alpha\alpha'\sigma}(\mathbf{k}), \\ G_{\alpha\alpha'\sigma}^>(\mathbf{k}; 0, 0) &= -i(\delta_{\alpha\alpha'} - \tilde{\rho}_{\alpha\alpha'\sigma}(\mathbf{k})), \end{aligned} \quad (7)$$

where $\tilde{\rho}_{\alpha\alpha'\sigma}(\mathbf{k})$ is the density matrix corresponding to the (uncorrelated) pre-quench equilibrium state.

In either setup, the KBEs (6) are solved with an in-house massively-parallel computer code (used also in Ref. [54]) based on a fifth-order predictor-corrector scheme. An equidistant time step of $\Delta t = 0.05$ was used, ensuring the convergence of all observables.

Generalized Kadanoff-Baym ansatz

The generalized Kadanoff-Baym ansatz (GKBA) [38] reduces the KBEs (6) to an equation of motion for the density matrix

$$\frac{d}{dt} \rho(\mathbf{k}; t) = -i [\mathbf{h}^{\mathbf{MF}}(t), \rho(\mathbf{k}; t)] - \mathbf{I}(\mathbf{k}, t), \quad (8)$$

where the collision term $\mathbf{I}(\mathbf{k}, t)$ is defined by

$$\mathbf{I}(\mathbf{k}, t) = [\mathbf{\Sigma}(\mathbf{k}) * \mathbf{G}(\mathbf{k})]^<(t, t) + \text{h. c.} \quad (9)$$

The time off-diagonal SPGF required for computing the collision integral (9) are reconstructed by the GKBA

$$\begin{aligned} -i\mathbf{G}^{\gtrless}(\mathbf{k}; t, t') &= \mathbf{G}^{\mathbf{R}}(\mathbf{k}; t, t') \mathbf{G}^{\gtrless}(\mathbf{k}; t, t') \\ &- \mathbf{G}^{\gtrless}(\mathbf{k}; t, t') \mathbf{G}^{\mathbf{A}}(\mathbf{k}; t, t'). \end{aligned} \quad (10)$$

We employ the Hartree-Fock (HF) approximation to the retarded SPGF:

$$\begin{aligned} \mathbf{G}^{\mathbf{R}}(\mathbf{k}; t, t') &= -i\theta(t - t') \mathcal{T} \exp \left(\int_{t'}^t d\bar{t} \mathbf{h}^{\mathbf{HF}}(\mathbf{k}; \bar{t}) \right) \\ &\equiv -i\theta(t - t') \mathbf{U}(\mathbf{k}; t, t'), \end{aligned} \quad (11)$$

where $\mathbf{h}^{\mathbf{HF}}(\mathbf{k}; \bar{t})$ denotes the mean-field HF Hamiltonian, while \mathcal{T} stands for the time-ordering symbol. The time-evolution operator $\mathbf{U}(\mathbf{k}; t, t')$ defined by Eq. (11) is computed using the semi-group property $\mathbf{U}(\mathbf{k}; t_n + \Delta t, t_j) = \mathbf{U}(\mathbf{k}; t_n +$

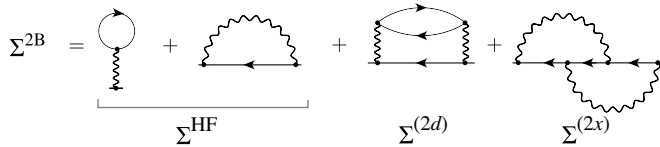


FIG. 5. Feynmann diagrams representing the second-Born approximation, consisting of the Hatree-Fock (first two diagrams), direct (third diagram) and exchange (last diagram) contribution.

$\Delta t, t_n) \mathbf{U}(\mathbf{k}; t_n, t_j)$ on a uniform mesh of time points $t_n = n\Delta t$. The propagator $\mathbf{U}(\mathbf{k}; t_n + \Delta t, t_n)$ is computed using the fourth-order commutator-free matrix-exponential method [55]. The GKBA equation (10) is solved using an in-house highly accurate computer code. A fixed time step $\Delta t = 0.05$ was used in all calculations.

Self-energy: second-Born approximation

All results in the main text have been obtained within the second-Born approximation (2BA). The corresponding diagrammatic representation is shown in Fig. 5.

Using the standard Feynmann rules [31], the diagrams for the 2BA have been cast into mathematical expressions on the Kadanoff-Baym contour and implemented in our computer codes. A general explicit expression in the Wannier representation can be found, for instance, in Ref. [56].

For nonlocal interactions, however, the large computational effort to treat the exchange diagram prevents us from employing the full 2BA in this case. Therefore, we have omitted $\Sigma^{(2x)}$ in the treatment of the Chern insulators with nonlocal interactions. For all other cases, we have confirmed that not including the exchange diagrams leads to very small quantitative changes. Hence, all statements in the main text on thermalization still remain valid. Note that even without including the exchange diagram, the resulting 2BA is still energy conserving.

Appendix: Scaling of purity gap closing

In the main text, we have discussed the purity gap closing characterized by the critical time t_{crit} . In order to investigate the dependence on the interaction, we have computed t_{crit} for additional values of the interaction strength for both the Chern insulator with local interactions only and including nonlocal interactions. The result is presented in Fig. 6.

Linear regression of $\log(t_{\text{crit}})$ as a function of $\log(V)$ shows that in the scenario with or without nonlocal interactions the critical time approximately scales as $\sim V^{-3/2}$. Interestingly, long-time relaxation times scale as $\sim V^{-2}$; hence, the time scale of the purity gap closing is different from thermalization and more related to dephasing effects.

Appendix: Calculation of the equilibrium Hall conductance

In order to investigate if the steady-state Hall conductance discussed in the main text corresponds to thermal equilibrium, we computed the equilibrium Hall conductance as a function of temperature. Following Ref. [40], we have prepared the initial density matrix $\rho_\sigma(\mathbf{k}, t = 0)$ with respect to the topologically nontrivial post-quench Hamiltonian including interactions on the mean-field level. Propagating using the GKBA while adiabatically switching on the 2BA self-energy yields a correlated initial state $\rho_\sigma(\mathbf{k}, t_{\text{switch}})$. Applying the probe electric field $E_y(t) = F_0(1 - e^{-(t-t_{\text{switch}})/\tau_0})$ ($E_y(t) = 0$ for $t < t_{\text{switch}}$) after the interactions are switched on then yields the equilibrium Hall conductance via $\sigma_{xy} = \lim_{t \rightarrow \infty} J_x(t)/F_0$. This procedure is performed for a set of inverse temperatures β . Repeating the adiabatic switching procedure without probe field leads to a constant total energy E_{tot} , which yields the temperature dependence of E_{tot} . The function $E_{\text{tot}}(\beta)$ is then used to determine the effective temperature T_{eff} . The adiabatic switching was realized using the double-exponential switch-on function from ref. [56], using a time interval of $t_{\text{switch}} = 40$.

Within the full KBE treatment, on the other hand, the preparation of a correlated initial state in thermal equilibrium is accomplished by solving the Dyson equation for the Matsubara SPGF $\mathbf{G}^M(\mathbf{k}; \tau)$. The total energy $E_{\text{tot}}(\beta)$ is computed via the Galitskii-Migdal formula [31]. The time evolution in the presence of the probe field $E_y(t) = F_0(1 - e^{-(t/\tau_0)})$ is then obtained by solving the full set of the KBEs (6).

Figure 7 shows the spin Hall conductance of the \mathbb{Z}_2 insulator in thermal equilibrium, comparing the full KBE and the GKBA treatment. The agreement is very good for smaller β (higher temperature, that is) and weaker interactions, while deviations become apparent for low temperature and stronger interaction. In particular, the full KBE treatment recovers the limit $\sigma_{xy}^s \rightarrow e^2/h$ for $\beta \rightarrow \infty$. This is consistent with the fact that the topological properties can not be altered by (weak) electron-electron interactions. In contrast, the GKBA does not reproduce this limit correctly. Nevertheless, since the effective temperatures in the quench setup studied in the main text are

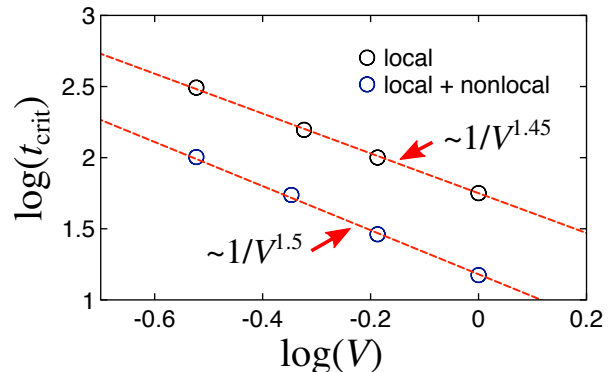


FIG. 6. Double-logarithmic plot of the critical time of the purity gap closing as function of the interaction strength.

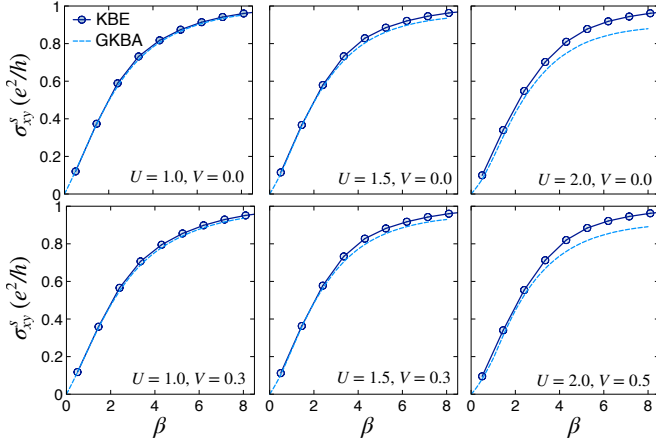


FIG. 7. Hall conductance of the spinfull \mathbb{Z}_2 insulator in thermal equilibrium as a function of the inverse temperature β for different values of the local interaction parameters U and V .

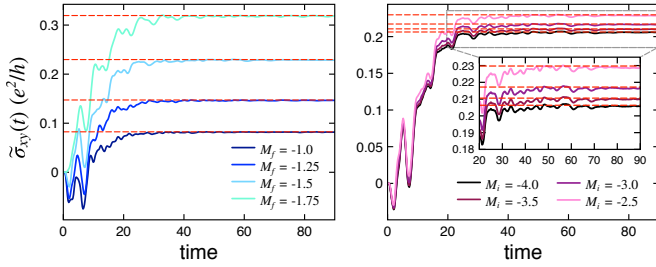


FIG. 8. Nonequilibrium (spin) Hall conductance of the spinfull \mathbb{Z}_2 insulator for the same setup as in the main text. In the left panel, $M_i = -3.5$, while $M_f = -1.5$ for the panel on the right-hand side. The red-dashed lines indicate the corresponding thermal equilibrium.

quite high (typically $\beta \sim 1$ to $\beta \sim 2$), the GKBA provides an accurate description.

Appendix: Dependence on pre- and post-quench gap parameter

Figure 8 shows the nonequilibrium Hall conductance $\tilde{\sigma}_{xy}(t)$ of the spin Chern insulator in analogy to the result in the main text for different values of the pre- (M_i) and post-quench (M_f) mass parameter. The parameters are the same as in the main text. The Coulomb interaction has been fixed to $U = 1.5$, $V = 0.0$. We have used the GKBA to obtain the results in Fig. 8.

As Fig. 8 demonstrates, the nonequilibrium Hall conductance approaches the respective thermal equilibrium value for all parameters. Inspecting the dependence on the initial mass parameter M_i (right-hand panel in Fig. 8), one finds a quite weak variation. This indicates that the gap size of the pre-quench band insulator plays only a minor role, since the band hybridization can be neglected. In contrast, the dependence on the post-quench gap parameter M_f (left-hand panel in Fig. 8) is much more pronounced. One finds an increasing Hall conductance with M_f approaching the phase boundary $M_f = -2$.

This can be understood by the amount of energy injected by the quench, which is minimal for $M_f \rightarrow -2$. Therefore, the steady-state Hall conductance is the largest for $M_f = -1.75$. This dependence explains the dependence of σ_{xy}^s of the spin Chern insulator on U discussed in the main text: right after quench, the effective mean-field Hamiltonian $\mathbf{h}_{\uparrow,\downarrow}^{\text{HF}}(\mathbf{k})$ becomes

$$\mathbf{h}_{\uparrow,\downarrow}^{\text{HF}}(\mathbf{k}) = \mathbf{h}_{\uparrow,\downarrow}(\mathbf{k}) + U \begin{pmatrix} n_E + \frac{1}{2} & 0 \\ 0 & n_E - \frac{1}{2} \end{pmatrix}. \quad (12)$$

Since the lower band of the pre-quench band insulator is predominantly consisting of the E -orbital, the occupation $n_E \approx 1$, thus $\mathbf{h}_{\uparrow,\downarrow}^{\text{HF}}(\mathbf{k}) \approx \mathbf{h}_{\uparrow,\downarrow}(\mathbf{k}) + \frac{U}{2}\sigma_z$, corresponding to the free Hamiltonian $\mathbf{h}_{\uparrow,\downarrow}(\mathbf{k})$ with $M \rightarrow M - U/2$. Hence, increasing U results in an effective post-quench mass parameter deeper in the topological phase, and thus a larger energy injection and a reduced steady-state Hall conductance.

- [1] M. Aidelsburger, M. Atala, M. Lohse, J. T. Barreiro, B. Paredes, and I. Bloch, Phys. Rev. Lett. **111**, 185301 (2013).
- [2] H. Miyake, G. A. Siviloglou, C. J. Kennedy, W. C. Burton, and W. Ketterle, Phys. Rev. Lett. **111**, 185302 (2013).
- [3] G. Jotzu, M. Messer, R. Desbuquois, M. Lebrat, T. Uehlinger, D. Greif, and T. Esslinger, Nature **515**, 237 (2014).
- [4] Z. Wu, L. Zhang, W. Sun, X.-T. Xu, B.-Z. Wang, S.-C. Ji, Y. Deng, S. Chen, X.-J. Liu, and J.-W. Pan, Science **354**, 83 (2016).
- [5] N. Fläschner, B. S. Rem, M. Tarnowski, D. Vogel, D.-S. Lühmann, K. Sengstock, and C. Weitenberg, Science **352**, 1091 (2016).
- [6] N. Goldman, J. C. Budich, and P. Zoller, Nature Physics **12**, 639 (2016).
- [7] Y. H. Wang, H. Steinberg, P. Jarillo-Herrero, and N. Gedik, Science **342**, 453 (2013).
- [8] J. W. McIver, B. Schulte, F.-U. Stein, T. Matsuyama, G. Jotzu, G. Meier, and A. Cavalleri, arXiv:1811.03522 [cond-mat] (2018).
- [9] X. Chen, Z.-C. Gu, and X.-G. Wen, Physical Review B **82**, 155138 (2010).
- [10] D. T. Tran, A. Dauphin, A. G. Grushin, P. Zoller, and N. Goldman, Science Advances **3**, e1701207 (2017).
- [11] M. Schüler and P. Werner, Phys. Rev. B **96**, 155122 (2017).
- [12] D. T. Tran, N. R. Cooper, and N. Goldman, Phys. Rev. A **97**, 061602 (2018).
- [13] M. Caio, N. Cooper, and M. Bhaseen, Phys. Rev. Lett. **115**, 236403 (2015).
- [14] H. Deghani and A. Mitra, Phys. Rev. B **92**, 165111 (2015).
- [15] H. Deghani, T. Oka, and A. Mitra, Phys. Rev. B **91**, 155422 (2015).
- [16] P. Wang, M. Schmitt, and S. Kehrein, Phys. Rev. B **93**, 085134 (2016).
- [17] Y. Hu, P. Zoller, and J. C. Budich, Phys. Rev. Lett. **117**, 126803 (2016).
- [18] M. Schmitt and P. Wang, Phys. Rev. B **96**, 054306 (2017).
- [19] L. Ulčakar, J. Mravlje, A. Ramšak, and T. Rejec, Phys. Rev. B **97**, 195127 (2018).
- [20] L. Peralta Gavensky, G. Usaj, and C. A. Balseiro, Phys. Rev. B **98**, 165414 (2018).

- [21] Y. Xu and Y. Hu, arXiv:1807.09732 [cond-mat, physics:quant-ph] (2018).
- [22] S. Wolff, A. Sheikhan, and C. Kollath, Phys. Rev. A **94**, 043609 (2016).
- [23] J. Berges, S. Borsányi, and C. Wetterich, Phys. Rev. Lett. **93**, 142002 (2004).
- [24] M. Moeckel and S. Kehrein, Phys. Rev. Lett. **100**, 175702 (2008).
- [25] M. Eckstein, M. Kollar, and P. Werner, Phys. Rev. Lett. **103**, 056403 (2009).
- [26] M. Marcuzzi, J. Marino, A. Gambassi, and A. Silva, Phys. Rev. Lett. **111**, 197203 (2013).
- [27] L. D'Alessio, Y. Kafri, A. Polkovnikov, and M. Rigol, Advances in Physics **65**, 239 (2016).
- [28] A. Kruckenhauser and J. C. Budich, arXiv:1712.02440 [cond-mat, physics:quant-ph] (2017).
- [29] A. Stan, N. E. Dahlen, and R. v. Leeuwen, J. Chem. Phys. **130**, 224101 (2009).
- [30] K. Balzer and M. Bonitz, *Nonequilibrium Green's Functions Approach to Inhomogeneous Systems* (Springer, 2012).
- [31] G. Stefanucci and R. v. Leeuwen, *Nonequilibrium Many-Body Theory of Quantum Systems: A Modern Introduction* (Cambridge University Press, 2013).
- [32] B. A. Bernevig, T. L. Hughes, and S.-C. Zhang, Science **314**, 1757 (2006).
- [33] C.-L. Hung, V. Gurarie, and C. Chin, Science **341**, 1213 (2013).
- [34] P. Makotyn, C. E. Klauss, D. L. Goldberger, E. A. Cornell, and D. S. Jin, Nature Physics **10**, 116 (2014).
- [35] H. Aoki, N. Tsuji, M. Eckstein, M. Kollar, T. Oka, and P. Werner, Rev. Mod. Phys. **86**, 779 (2014).
- [36] K. Balzer, N. Schlünzen, and M. Bonitz, Phys. Rev. B **94**, 245118 (2016).
- [37] M. Schüler and Y. Pavlyukh, Phys. Rev. B **97**, 115164 (2018).
- [38] P. Lipavsky, V. Spicka, and B. Velicky, Phys. Rev. B **34**, 6933 (1986).
- [39] The GKBA reduces the original KBEs, which constitute the a set of two-time integro-differential equations with memory, to a single-time non-Markovian equation.
- [40] S. Latini, E. Perfetto, A.-M. Uimonen, R. van Leeuwen, and G. Stefanucci, Phys. Rev. B **89**, 075306 (2014).
- [41] E. Perfetto, A.-M. Uimonen, R. van Leeuwen, and G. Stefanucci, Phys. Rev. A **92**, 033419 (2015).
- [42] E. Perfetto, D. Sangalli, A. Marini, and G. Stefanucci, J. Phys. Chem. Lett. **9**, 1353 (2018).
- [43] E. V. n. Boström, A. Mikkelsen, C. Verdozzi, E. Perfetto, and G. Stefanucci, Nano Lett. **18**, 785 (2018).
- [44] S. Diehl, E. Rico, M. A. Baranov, and P. Zoller, Nature Physics **7**, 971 (2011).
- [45] C.-E. Bardyn, L. Wawer, A. Altland, M. Fleischhauer, and S. Diehl, Phys. Rev. X **8**, 011035 (2018).
- [46] In our case, the gap closing of $\mathbf{h}_{\text{aux}}(\mathbf{k}; t)$ occurs at the Γ point. In the noninteracting system in equilibrium, $\mathbf{h}_{\text{aux}}(\mathbf{k}) = \mathbf{h}(\mathbf{k})$, hence the gap closing is equivalent to $M = -2$.
- [47] The index C_i is identical to the Chern number C of \mathbf{h}_{aux} in equilibrium.
- [48] Supplemental material, available online.
- [49] In the thermodynamic limit, $C_i(t)$ is identical to $C_{\text{inst}}(t)$. The pronounced finite-size effects for $V = 0.65$ since the very weak dephasing leads to the deviations in Fig. 2 (c)–(d).
- [50] J. C. Budich, B. Trauzettel, and G. Sangiovanni, Phys. Rev. B **87**, 235104 (2013).
- [51] This manifestation of the topological invariant is unaffected by the interaction [57].
- [52] N. Schlünzen, J.-P. Joost, F. Heidrich-Meisner, and M. Bonitz, Phys. Rev. B **95**, 165139 (2017).
- [53] We choose $f(\tau) = 10\tau^3 - 15\tau^4 + 6\tau^5$ for $\tau \in [0, 1]$.
- [54] M. Schüler, Y. Murakami, and P. Werner, Phys. Rev. B **97**, 155136 (2018).
- [55] A. Alvermann and H. Fehske, J. Comput. Phys. **230**, 5930 (2011).
- [56] N. Schlünzen and M. Bonitz, Contributions to Plasma Physics **56**, 5 (2016).
- [57] J. Fröhlich and P. Werner, EPL (Europhysics Letters) **101**, 47007 (2013).